

Interferometry on the compact toroid formation experiments at Phillips Laboratory

E. L. Ruden, B. W. Mullins, and M. E. Dearborn
High Energy Plasma Division, Phillips Laboratory, Kirtland Air Force Base, New Mexico 87117-6008

S. K. Coffey
R&D Associates, Alexandria, Virginia 22314

(Received 4 March 1991; accepted 20 March 1992)

Interferometric measurements of the line-averaged free electron density of plasma compact toroids as part of preliminary toroid formation experiments are presented. These experiments are in preparation for compact toroid acceleration experiments to be performed at Phillips Laboratory's High Energy Plasma Division. The primary instrument used was a Michelson (double pass) interferometer operating with a HeNe laser at a wavelength of 633 nm. Density measurements of hydrogen and argon plasmas are correlated with magnetic field and spectroscopic measurements to characterize the toroid mass, velocity, and impurity distribution.

I. INTRODUCTION

The High Energy Plasma Division of Phillips Laboratory has completed initial experiments on the formation of compact toroids (CT's) confined between two coaxial conductors using both hydrogen and argon plasmas. These experiments are the first stage in an overall experiment known as MARAUDER (Magnetically Accelerated Rings to Achieve Ultrahigh Density Energy and Radiation), which is an energy upgrade of the RACE (Ring Acceleration Experiment) effort at Lawrence Livermore National Laboratory (LLNL).¹ The goal is to accelerate 0.1–10 mg CT's to 5 MJ of kinetic energy by driving current axially up one confining coaxial conductor, radially behind the CT, and down the other coaxial conductor, as in a coaxial railgun.

In this paper we focus on results from interferometric data and complementary measurements taken as part of the MARAUDER formation experiments. Interferometry was performed primarily with a HeNe laser with a wavelength $\lambda=0.633 \mu\text{m}$. Correlating the interferometric results with those from magnetic probes and an optical multichannel analyzer (OMA) provide estimates of basic CT properties such as mass, velocity, and axial density distribution. An independent estimate of the mass of the total injected neutral gas from which the CT is formed is provided for comparison with the interferometric estimate of CT mass. A supplementary general overview of the experiment is provided elsewhere.^{2,3} Sufficient details of the overall experiment are provided here to facilitate interpretation of the presented results and for continuity.

II. THEORETICAL CONSIDERATIONS

The interferometric results presented are derived from measurements of the plasma induced phase shift ϕ_p (radians) of a laser beam probing across the diameter of the CT as it moves axially past an observation port. The temperatures, densities, and magnetic field intensities encountered

are sufficiently low for the plasma free electron density averaged over the laser beam path L to be accurately determined by^{4,5}

$$\bar{n}_e \equiv \frac{1}{L} \int_0^L n_e dL = \frac{3.55 \times 10^{12}}{pL\lambda} \phi_p \quad (\text{cgs}). \quad (1)$$

Here $p=2$ is the number of passes the laser makes through the plasma.

If we assume that the plasma is azimuthally symmetric and confined between the inner and outer conductors at radii $R_1=44.8 \text{ cm}$ and $R_2=62.5 \text{ cm}$, and assign $L=2(R_2-R_1)$, then $\bar{n}_e=\bar{n}_e(z,t)$, as derived from ϕ_p in Eq. (1), may be interpreted as the radial average of $n_e=n_e(r,z,t)$ between R_1 and R_2 at $z=z_p$

$$\bar{n}_e = (R_2 - R_1)^{-1} \int_{R_1}^{R_2} n_e(r, z, t) dr. \quad (2)$$

The assumption of axial symmetry of the CT is fairly well justified by magnetic probe measurements at different azimuthal positions in the expansion region.^{2,3} The confinement assumption is justified by microwave transmission measurements made transversely through the diagnostic ports, as discussed in Sec. III.

The total number of free electrons in the CT is

$$N_e = \int_{z_1}^{z_2} \int_{R_1}^{R_2} 2\pi r n_e(r, z, t) dr dz, \quad (3)$$

where z_1 and z_2 are the axial extremes of the CT. For MARAUDER, the r cofactor in the integrand varies little enough between R_1 and R_2 to replace it with $(R_1+R_2)/2$, resulting in

$$N_e \approx \pi(R_2^2 - R_1^2) \int_{z_1}^{z_2} \bar{n}_e(z, t) dz. \quad (4)$$

Unfortunately, the interferometer is only configured to measure \bar{n}_e vs t for the fixed axial position $z=z_p$. However, if we assume that the plasma passes the interferometric

probe beam with a constant and uniform axial velocity v_z , then fluid continuity and Eq. (4) imply

$$N_e \approx \pi(R_2^2 - R_1^2)v_z \int_{t_1}^{t_2} \bar{n}_e(z_p, t) dt, \quad (5)$$

where t_1 and t_2 are the times when the forward and rear edge of the CT pass z_p .

The assumptions that the CT plasma moves at a constant and uniform velocity as it passes z_p is probably the greatest source of error in estimating the total free electron load of the CT. An estimate of v_z is obtained from the relative timing of reference points on the magnetic field signal of the CT as it passes two magnetic probes at z_p and 13.7 cm down range of z_p . The time intervals between magnetic probe reference points, such as the peak amplitude, and the ascending and descending half peak amplitude of the various magnetic field components (see Fig. 6, for example), indicate that v_z may actually drop by as much as a factor of 2 at z_p during the time the CT passes. Therefore, any N_e estimate derived from Eq. (5) will have a significant degree of uncertainty.

An estimate of the CT mass M can be obtained from the N_e estimate if the mean ion mass \bar{m}_i , and ionization level \bar{Z} (including impurities) can be established. Given net charge neutrality,

$$M = \bar{m}_i N_e / \bar{Z}. \quad (6)$$

Information about \bar{m}_i and \bar{Z} are supplied by an optical multichannel analyzer (OMA), which records the optical emission spectrum for a specified (gated) time interval.^{2,6,7} A temperature estimate of 2–4 eV is available⁶ for the H data presented, based on the local thermodynamic equilibrium (LTE) model.⁸ It is reasonable to assume that the H is mostly ionized ($\bar{Z} \approx 1$) in this temperature range for the density magnitudes involved.⁹ The Ar⁺ emission lines are observed, along with an unknown percentage of H and C contaminants, for Ar discharges. The Ar⁺ line ratios indicate that the electron temperature is 3–4 eV,⁷ based on the collisional radiative equilibrium (CRE) model.¹⁰ $\bar{Z} = 1-2$ in this temperature range, according to this model.

The CT plasma source is a neutral gas (either H₂ or Ar) injected into the CT formation gun region by 60 fast gas valves, as discussed in Sec. III. An estimate of the mass M_0 of the neutral gas injected by the gas valves between time $t=0$ (valve trigger) and $t=T_1$ (gun bank trigger) is available for comparison with the interferometric estimate of M . The gas injection time scale is too long for a significant amount of gas injected after $t=T_1$ to be incorporated into the CT. The M_0 estimate is derived from piezoelectric probe¹¹ measurements of the pressure versus time of the gas jet from a single nozzle. The probe is placed with its 0.5 cm diam pressure sensitive surface about 1 cm from the nozzle orifice. Assuming that the gas jet pressure signal V_p is proportional to the gas flow rate,

$$M_0 = M_{\text{tot}} \frac{\int_0^{T_1} V_p dt}{\int_0^{\infty} V_p dt}. \quad (7)$$

Here, M_{tot} is the total mass that all 60 valves inject by the time they close. The value of M_{tot} is determined by firing a single valve into a small vacuum chamber of known volume, measuring the pressure change, and applying the ideal gas law. The pressure is measured with a thermocouple gauge and is corrected for a gas species using absolute pressure calibration data supplied by the vendor.¹²

III. EXPERIMENTAL

A schematic of MARAUDER, as configured for the formation experiments, is illustrated in Fig. 1. The basic firing sequence is as follows.

(1) A slowly rising, principally radial, magnetic field is imposed on the upper gun region by external magnetic field coils both interior and exterior to the gun region, as shown. The coils are supplied by a capacitor bank charged to voltage V_B .

(2) When the radial magnetic field reaches its peak value, neutral gas (either H₂ or Ar) of mass M_0 is injected into the gun region at axial position $z \equiv 0$ by 60 fast gas valves distributed evenly around the circumference.

(3) Voltage from the plasma gun capacitor bank (charged to voltage V_G) is applied between the inner and outer conductors of the gun region after a time T_1 from the gas valve trigger.

(4) The injected gas breaks down from the applied voltage and becomes a highly conducting plasma, thereby “freezing” in the radial magnetic field in addition to the azimuthal (toroidal) field produced by the current flowing from the gun bank and across the plasma.

(5) The $\mathbf{J} \times \mathbf{B}$ forces eject the plasma into the expansion region, stretching the radial field lines into a poloidal configuration, as illustrated in Fig. 2.

(6) The poloidal field lines resistively reconnect behind the plasma, releasing into the expansion region a CT with closed poloidal and toroidal magnetic field lines and with a mean axial velocity v_z .

The reader is referred to Refs. 2 or 3 for quantitative information on time scales, physical dimensions, field intensities, etc.

Interferometric data was taken with the laser probe beam traversing a diameter located at axial position $z = z_p = 36$ cm (16 cm beyond the gun region), as illustrated in Fig. 1. A schematic of the optical path is shown in Fig. 3. The system utilizes a Michelson geometry with a reference path folded, so as to be contained on a 122 cm by 61 cm optical breadboard. A return mirror for the plasma probe beam is mounted 4.6 m from the main assembly. After being recombined back on the optical board, the interfering probe and reference beams are focused into an optical fiber. The intensity modulated light is transmitted to a rf enclosure, where its intensity is measured by a photomultiplier. The phase shift ϕ_p of the probe beam resulting from the plasma is then derived from the sinusoidal relationship between the measured light intensity and ϕ_p .¹³ The effect on the interference signal of stray light reflected from the fiber optic and laser aperture surfaces, which could cause a standing wave to be set up in the interferometer, may be neglected because of the significant beam diver-

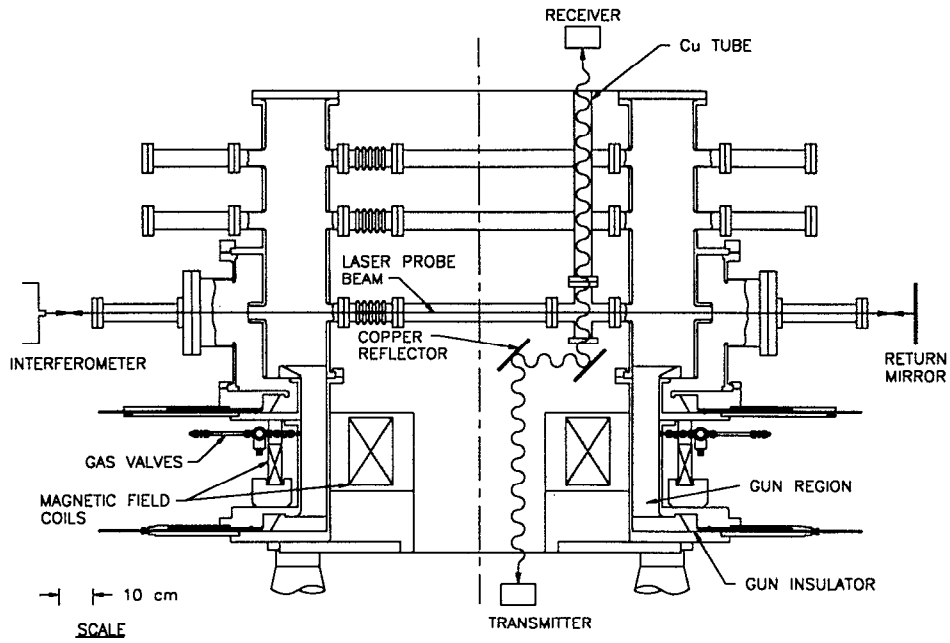


FIG. 1. Schematic of MARAUDER formation experiment. The laser interferometer probe beam is shown at the axial position for the presented data. The radiation path of the microwave interferometer for the cross-tube probe is also shown.

gence due to the long (9.2 m) optical path lengths of the probe and reference beams.

Detector noise limits the detection threshold of the interferometer to about $3 \times 10^{14} \text{ cm}^{-3}$. Another source of error results from a $\sim 10 \text{ Hz}$ variation in the detector sig-

nal amplitude at maximum and minimum interference. These reference values, recorded after each shot, are used to normalize the signal before performing the arcsine operation necessary to determine phase shift. The reference variation results in an absolute uncertainty in density of

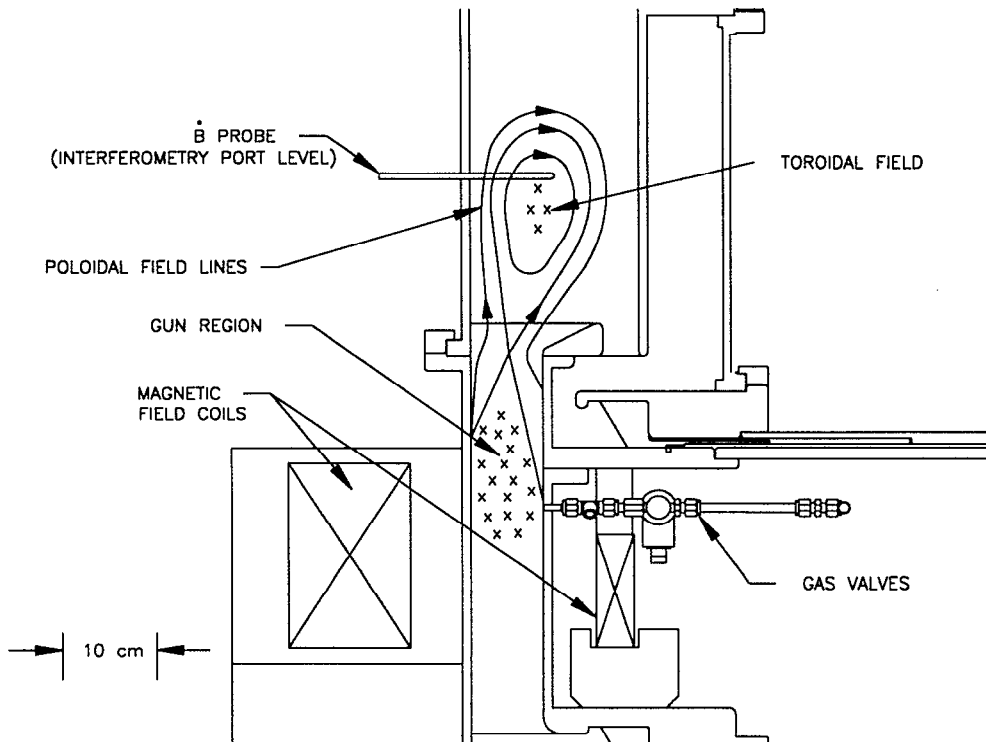


FIG. 2. Conceptual schematic of the CT plasmoid as it is ejected from the gun. The position of the magnetic probes for the presented data is shown for reference.

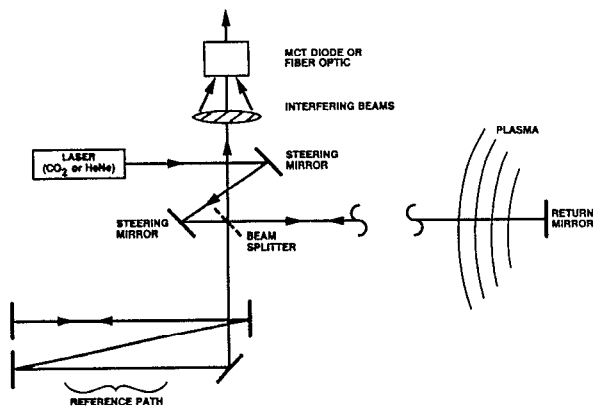


FIG. 3. Interferometer optical path (Michelson geometry with a folded reference path).

about 10%. The variation results from vibration of the interferometer support structure. This vibration also causes a time-dependent phase shift, but at a frequency too low to interfere with interpretation of the phase shift due to the plasma.

A potential contributing factor to \bar{n}_e is plasma entering the laser probe access tubes interior to R_1 and exterior to R_2 . If significant, this contribution would render Eq. (2) invalid and complicate data interpretation. This possibility is ruled out as a significant factor by measurements from a 3.33 mm wavelength microwave interferometric system. This system, shown schematically in Fig. 4, consists of a 250 mW, 90.9 GHz transmitter and a receiver. The receiver mixes the signal from the transmitter with its own local oscillator, so the resultant output varies by an amount proportional to the sine of the phase shift due to the plasma. The transmitter and receiver oscillators are phase locked to independent 100 MHz crystal oscillators to avoid the noise problems of any electrical connection between the units. The frequency difference between the two crystal oscillators can be maintained to within 1 Hz. This provides, after frequency multiplication, a mixer output base-

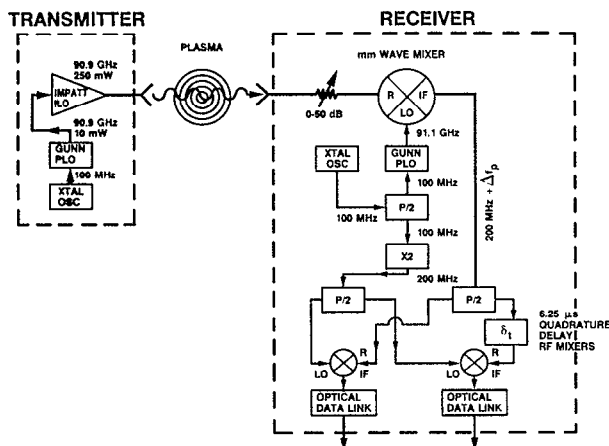


FIG. 4. Microwave interferometer schematic.

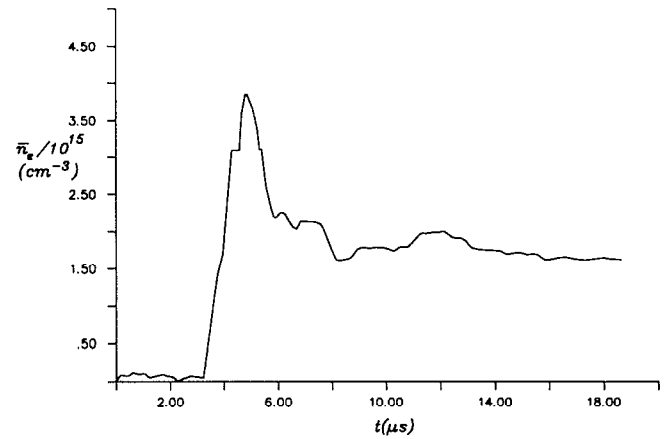


FIG. 5. Here \bar{n}_e vs t for the H_2 plenum with $P=1.12 \times 10^6$ Pa, $T_1=425$ μ sec, $V_B=2.8$ kV, and $V_G=60.2$ kV (shot No. 05169005).

line of about 1 kHz (effectively dc for the time scales of interest).

The microwave system was fielded as illustrated in Fig. 1. The sensitivity of an interferometer to n_e , as implied by Eq. (1), is proportional to the radiation wavelength (5260 times greater for the microwave system than for the HeNe laser). These measurements indicate that the n_e densities entering the interior tube do not exceed $\sim 10^{13}$ cm^{-3} for at least 30 μ sec after the time of gun current trigger. Comparison to the densities and time scales of interest discussed in Sec. IV indicate that plasma entering the tubes should be of no concern.

IV. Results

A. H_2 plenum

Figure 5 shows the interferometrically derived \bar{n}_e for a shot for which the valve plenum gas is H_2 at a pressure of $P=1.12 \times 10^6$ Pa (all pressures are absolute). Time $t=0$ for the abscissa corresponds to the onset of gun current. Referring to the parameters defined in Sec. III, other parameters for this shot are $T_1=425$ μ sec, $V_B=2.8$ kV, and $V_G=60.2$ kV. The magnitude of \bar{n}_e rises to a peak at $t=4.5$ μ sec and then falls to a plateau at $t \approx 6.0$ μ sec. Spectroscopic data^{2,6} taken at $z=z_p$ indicate that the initial peak consists primarily of hydrogen, while the plateau plasma contains both hydrogen and carbon. The initial peak records the passage of the CT while the plateau is due to a trailing plasma heavily contaminated by, if not primarily consisting of, hydrogen and carbon ions originating from hydrocarbons deposited on the vacuum chamber walls. These deposits, visible to the eye as a sooty film, apparently originate from the polyethylene gun insulator (Fig. 1). This insulator invariably flashes over and self-crowbars at some time after maximum gun current, liberating hydrocarbons that contaminate subsequent shots.

Figure 6 shows, for this shot, plots of the gun current, as measured with a B_θ probe at the back of the gun, and the three components of \mathbf{B} at $z=z_p$, and $r=53.7$ cm (midway between R_1 and R_2), as measured with probes at different azimuthal positions. The gun current plateau at $t \approx 5$ μ sec

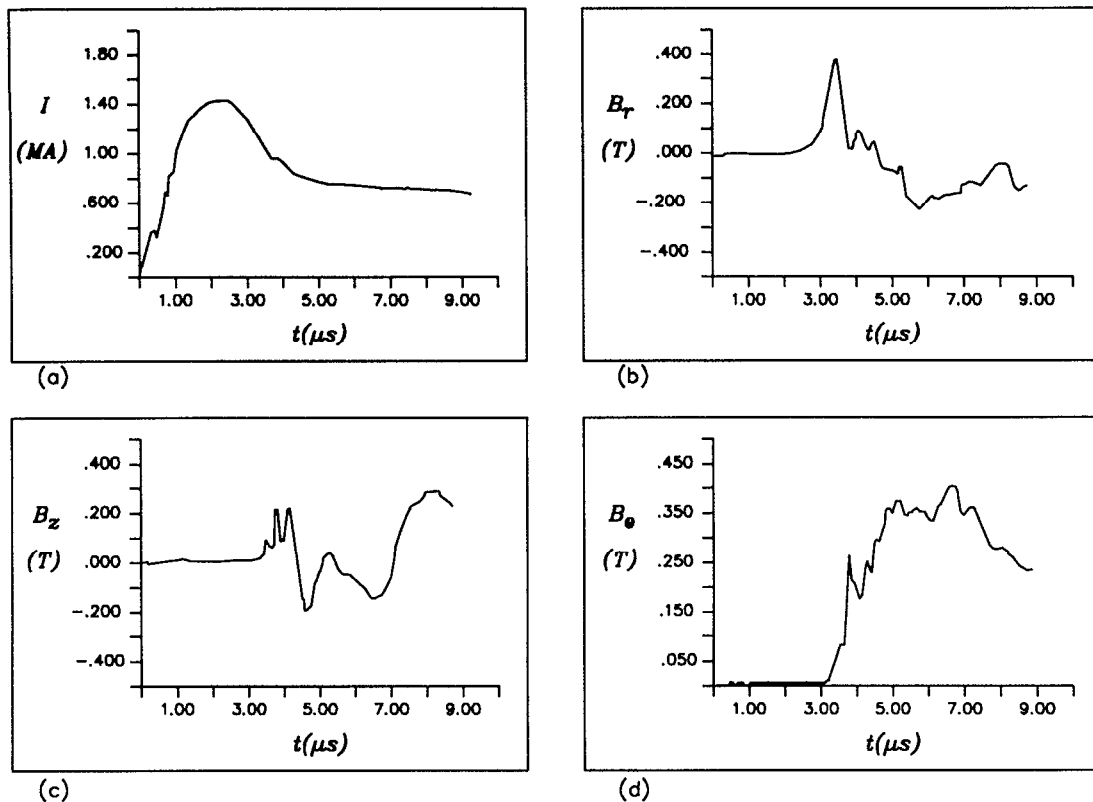


FIG. 6. (a) Gun current and components of the \mathbf{B} field at $z=z_p$, $r=53.7$ cm; (b), (c), and (d), for shot No. 05169005.

results from the insulator crowbar. A significant reference point on the B_r trace is the time at which it reverses sign. The B_r reversal is the signature of the poloidal magnetic field centroid passing $z=z_p$ and is temporally well correlated with the peak in \bar{n}_e . The plateau of the B_θ trace results from axial current behind the CT (by Ampère's law) ejected from the gun, and is, as expected, temporally correlated with the falloff of the peak in \bar{n}_e .

The CT mass for the H_2 plenum shot shown is estimated by the method described in Sec. II [Eqs. (5) and (6)]. The first peak in the B_r signal provides a fairly reproducible reference point for application of the CT axial velocity v_z estimate discussed. Using $v_z = \Delta z / \Delta t$ for a set of B_r measurements at $z=z_p$ and $z=z_p + \Delta z$ ($\Delta z = 13.6$ cm), where Δt is the time interval between peak B_r at the two positions, one obtains $v_z \approx 1.2 \times 10^7$ cm/sec at $z=z_p$ for machine parameters similar to that of the H_2 data shown. We perform the time integral of \bar{n}_e from $t_1 = 3$ μsec to the first significant local minimum in \bar{n}_e at $t_2 = 8$ μsec . With this, Eq. (5) yields, for the total electron number, $N_e = 8.0 \times 10^{20}$. Assuming the CT consists primarily of a singly ionized hydrogen, as discussed in Sec. II, Eq. (5) yields $M = 1.34$ mg as the CT mass estimate.

The injected H_2 mass M_0 for our parameters is estimated by the method described in Sec. II [Eq. (7)]. Figure 7 shows the piezoelectric signal resulting from the gas jet of a valve charged with 1.12×10^6 Pa H_2 . Here, $t=0$ corresponds to the time at which the valve is triggered. With this trace, and the corresponding M_{tot} estimate derived

from the pressure change in the vacuum chamber following the valve firing, Eq. (7) gives $M_0 = 1.22$ mg.

B. Ar plenum

Figure 8 shows \bar{n}_e for a shot that uses Ar at 8.27×10^4 Pa as the plenum gas. It is often difficult to distinguish a clear CT peak isolated from the trailing plasma when Ar is used as a plenum gas. This may be at least partially due to a given mass of ionized Ar having fewer electrons than H in proportion to its relative atomic mass (gas injection

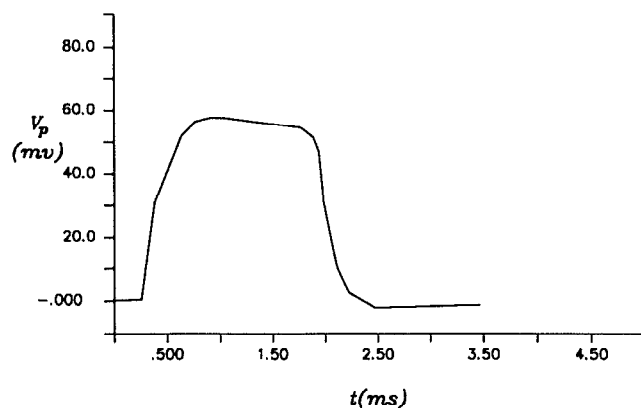


FIG. 7. Pressure signal versus time after trigger from one gas valve puffing on the piezoelectric probe located about 1 cm from the valve orifice (1.12×10^6 Pa H_2 plenum).

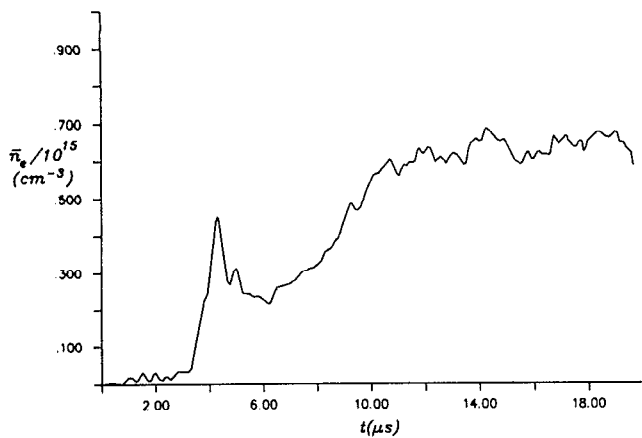


FIG. 8. Here \bar{n}_e vs t for Ar plenum with $P=8.27 \times 10^4$ Pa, $T_1=1000$ μ sec, $V_B=2.5$ kV, and $V_G=60.8$ kV (shot No. 05049008).

parameters were usually chosen to release ~ 1 mg into the gun). The data shown represents the lowest plenum pressure investigated as of this writing and yields the clearest interferometric CT signature available. Magnetic probe signals indicate, however, that for a much wider range of Ar plenum pressures, there is a qualitatively similar magnetic field structure as that shown above for H_2 (Ref. 2).

The magnetic probe estimate of the Ar CT velocity is $v_z \approx 1.2 \times 10^7$ cm/sec (similar to the H CT). We take the \bar{n}_e time integral from $t_1=3$ μ sec to $t_2=6$ μ sec (over the first peak in Fig. 8). If we assume \bar{m}_i is that of Ar and \bar{Z} is 1–2 for our interferometric mass estimate, discussed in Sec. II, Eq. (5) gives $N_e=5.4 \times 10^{19}$, and Eq. (6) gives $M=1.8$ –3.6 mg.

The piezoelectric probe estimate of the injected Ar mass for the plenum pressure and T_1 of the Ar data shown is 0.58 mg. A modification of the technique described in Sec. II is required for this estimate because the plenum pressure used (8.27×10^4 Pa) is too low for the piezoelectric probe to yield a clear V_p signal. Because of this, V_p as used in Eq. (7), is taken from a measurement for which the plenum pressure is 2.20×10^5 Pa. This is justified by the observation that the shape of V_p vs t varies little with plenum pressure in this pressure range. Increasing the plenum pressure results primarily in only the magnitude of V_p increasing, which has no effect on Eq. (7). The value of M_{tot} however, was measured accurately at 8.27×10^4 Pa using the thermocouple gauge.

V. DISCUSSION

For the H_2 data presented, there is substantial agreement in the estimates of injected gas mass and final CT mass. For the Ar data, though, the interferometric mass estimate significantly exceeds that of the injected mass. It is probable that when injecting low Ar masses the subsequent Ar particle number falls below that of the hydrocarbon contaminants, resulting in the discrepancy. The correlation is still good for the hydrogen CT results presented because of its much greater electron load when a comparable mass is injected.

The significance of the contaminant load to the experiment when acceleration is attempted depends to a great extent on whether it is confined by the magnetic field to the vicinity of the walls where it is formed, or becomes incorporated in the CT volume. Adding a substantial mass to the CT from C^+ and H^+ contaminants could significantly lower the final CT velocity achievable, and lower the mean atomic number of a nominally Ar plasma.

The interferometer, as fielded, cannot distinguish between wall and bulk plasma. It measures only the average e^- density along a diameter, and wall plasma can freely follow the magnetic field lines across the observation ports and contribute to the signal. Reentrant glass tubes through which the laser passes may be able to penetrate the wall plasma. If the magnetic field penetrates the tubes, it would be a barrier to the wall plasma. This technique is being investigated as of this writing to help discriminate between wall and bulk plasma.

It should be stressed that some of the approximations required for the interferometric CT mass estimate were of uncertain accuracy. In particular, the assumption of a constant CT velocity is not very accurate, as mentioned. Any conclusions about mass transport drawn from the presented data are, at best, tentative. More statistics of the relative agreement between the two mass estimates will be pursued during the next stage of the experiment when the CT is accelerated. It is expected that the interferometric mass estimate will be more reliable during acceleration since the CT will, by then, have completely broken away from the gun and the trailing plasma. This should result in a better defined CT velocity and density distribution.

- ¹C. L. Hartman and J. H. Hammer, Phys. Rev. Lett. **48**, 929 (1982).
- ²B. W. Mullins, J. H. Degnan, J. D. Beason, M. E. Dearborn, D. Dietz, J. L. Holmes, E. L. Ruden, D. W. Price, C. R. Sovinec, K. E. Hackett, G. Bird, S. K. Coffey, S. W. Seiler, G. F. Kiuttu, R. E. Peterkin, N. F. Roderick, and P. J. Turchi, submitted to Phys. Fluids B.
- ³J. H. Degnan, B. W. Mullins, J. D. Beason, M. E. Dearborn, D. Dietz, K. E. Hackett, J. L. Holmes, E. L. Ruden, D. W. Price, C. R. Sovinec, G. Bird, S. K. Coffey, S. W. Seiler, G. F. Kiuttu, R. E. Peterkin, N. F. Roderick, and P. J. Turchi, in *Physics of Alternate Magnetic Confinement Schemes*, edited by S. Ortolani and E. Sindoni (Società Italiana di Fisica, Bologna, Italy, 1991), p. 965.
- ⁴*Plasma Diagnostics*, edited by W. Lochte-Holtgreven (Elsevier, New York, 1968), p. 607.
- ⁵M. A. Heald and C. B. Wharton, *Plasma Diagnostics with Microwaves* (Wiley, New York, 1965), pp. 98, 121.
- ⁶G. F. Kiuttu and D. W. Price, Bull. Am. Phys. Soc. **35**, 2059 (1990).
- ⁷T. J. Englert, D. W. Price, and G. F. Kiuttu, Bull. Am. Phys. Soc. **36**, 2459 (1991).
- ⁸*Plasma Diagnostic Techniques*, edited by R. H. Huddleston and S. L. Leonard (Academic, New York, 1965), p. 222.
- ⁹D. L. Book, *NRL Plasma Formulary* (Naval Research Laboratory, Washington, DC, 1987), p. 41.
- ¹⁰R. H. Huddleston and S. L. Leonard, in Ref. 8, p. 203.
- ¹¹Integrated-Circuit Piezoelectric Transducer, PCB Piezo-tronics, Inc., Model No. 112A23.
- ¹²Series 316 Vacuum Gauge Controller Instruction Manual, Granville-Phillips Co., Manual catalog No. 316005, revised September 1988, p. 2.3.
- ¹³M. Born and E. Wolf, *Principles of Optics*, 5th ed. (Pergamon, Elmsford, NY, 1975), p. 259.